EFDA–JET–PR(07)03

T. Tala, Y. Andrew, K. Crombé, P.C. de Vries, X. Garbet, N. Hawkes, H. Nordman, K. Rantamäki, P. Strand, A. Thyagaraja, J. Weiland, E. Asp, Y. Baranov, C. Challis, G. Corrigan, A. Eriksson, C. Giroud, M.-D. Hua, I. Jenkins, H.C.M. Knoops, X. Litaudon, P. Mantica, V. Naulin, V. Parail, K.-D. Zastrow
and JET EFDA contributors

Toroidal and Poloidal Momentum Transport Studies in JET

Toroidal and Poloidal Momentum Transport Studies in JET

T. Tala[1], Y. Andrew[2], K. Crombé[3], P.C. de Vries[2], X. Garbet[4], N. Hawkes[2], H. Nordman[5], K. Rantamäki[1], P. Strand[5], A. Thyagaraja[2], J. Weiland[5], E. Asp[5], Y. Baranov[2], C. Challis[2], G. Corrigan[2], A. Eriksson[5], C. Giroud[2], M.-D. Hua[2], I. Jenkins[2], H.C.M. Knoops[6], X. Litaudon[4], P. Mantica[7], V. Naulin[8], V. Parail[2], K.-D. Zastrow[2] and JET EFDA contributors*

[1]Association EURATOM-Tekes, VTT, P.O. Box 1000, FIN-02044 VTT, Finland
[2]EURATOM/UKAEA Fusion Association, Culham Science Centre, Oxon. OX14 3DB, UK
[3]Department of Applied Physics, Ghent University, Belgium
[4]Association EURATOM-CEA, CEA/DSM/DRFC Cadarache, St Paul-Lez-Durance, France
[5]Association EURATOM-VR, Chalmers University of Technology, Göteborg, Sweden
[6]Eindhoven University of Technology, Dept. of Applied Physics, The Netherlands
[7]Istituto di Fisica del Plasma CNR-EURATOM, via Cozzi 53, 20125 Milano, Italy
[8]Association Euratom-Risø National Laboratory, DK-4000 Roskilde, Denmark
** See annex of M.L. Watkins et al, "Overview of JET Results ", (Proc. 21st IAEA Fusion Energy Conference, Chengdu, China (2006)).*

Preprint of Paper to be submitted for publication in
Nuclear Fusion

Abstract.
This paper reports on the recent studies of toroidal and poloidal momentum transport in JET. The ratio of the global energy confinement time to the momentum confinement is found to be close to $\tau_E/\tau_f = 1$ except for the low density or low collisionality discharges where the ratio is $\tau_E/\tau_f = 2–3$. On the other hand, local transport analysis of tens of discharges shows that the ratio of the local effective momentum diffusivity to the ion heat diffusivity is $\chi_f/\chi_i \approx 0.1–0.4$ rather than unity, as expected from the global confinement times and used often in ITER predictions. The apparent discrepancy in the global and local momentum versus ion heat transport can be at least partly explained by the fact that momentum confinement within edge pedestal is worse than that of the ion heat and thus, momentum pedestal is weaker than that of ion temperature. In addition, while the ion temperature profile shows clearly strong profile stiffness, the toroidal velocity profile does not exhibit stiffness, as exemplified here during a giant ELM crash. Predictive transport simulations with the self-consistent modelling of toroidal velocity using the Weiland model and GLF23 also confirm that the ratio $\chi_f/\chi_i \approx 0.4$ reproduces the core toroidal velocity profiles well and similar accuracy with the ion temperature profiles. Concerning poloidal velocities on JET, the experimental measurements show that the carbon poloidal velocity can be an order of magnitude above the neo-classical estimate within the ITB. This significantly affects the calculated radial electric field and therefore, the $E \Diamond B$ flow shear used for example in transport simulations. Both the Weiland model and GLF23 reproduce the onset, location and strength of the ITB well when the experimental poloidal velocity is used while they do not predict the formation of the ITB using the neo-classical poloidal velocity in time-dependent transport simulation. The most plausible explanation for the generation of the anomalous poloidal velocity is the turbulence driven flow through the Reynold's stress. Both CUTIE and TRB turbulence codes show the existence of an anomalous poloidal velocity, being significantly larger than the neo-classical values. And similarly to experiments, the poloidal velocity profiles peak in the vicinity of the ITB and is caused by flow due to the Reynold's stress.

1. INTRODUCTION

It is well known that the $E \times B$ flow shear is one of the major players in quenching turbulence [1]. As the $E \times B$ flow shear is linked to poloidal and toroidal velocities through E_r, understanding of momentum transport is one of the key elements to achieve high fusion performance and good confinement. In addition, toroidal rotation gives stability against beta-limiting resistive wall modes by making the stationary wall appear more conducting [2]. Furthermore, both toroidal and in particular poloidal velocities play a crucial role in affecting the triggering mechanisms of the transport barriers through $E \times B$ flow shear. Throughout the paper the following definitions for the two main quantities, E_r and $E \times B$ flow shear $\omega_{E \times B}$ are used:

$$E_r = \frac{1}{e z_i n_i} - \nu_{\theta,i} B_\phi + n_{\theta,i} B_\theta, \qquad \omega_{E \times B} = \frac{r}{q} \frac{\delta(q v_E / r)}{\delta r} \tag{1}$$

where Z_i is the charge number, n_i the density, p_i the pressure, $v_{\theta,i}$ the poloidal velocity and $v_{f,i}$ the toroidal velocity of the ion species i, v_E is the $E\times B$ velocity, q is the safety factor and B_ϕ and B_θ are toroidal and poloidal components of the magnetic field.

This paper reports on recent experimental and modelling studies of both toroidal and poloidal momentum transport on JET. The paper is organised as follows: all the analyses of toroidal rotation and toroidal momentum transport are discussed in section 2 and those ones of poloidal velocities in section 3. Section 2.1 is devoted to studies of the global toroidal momentum and energy confinement times. The local transport analysis of momentum and ion heat diffusivities is carried out in section 2.2. Moreover, the profile resiliency of toroidal velocity profile is compared to the one of the ion temperature. Predictive transport simulations with self-consistent treatment of toroidal momentum transport are presented in section 2.3. In section 3.1, the experimental results on the measurement of the carbon poloidal velocities in plasmas with strong ITBs are shown and the comparison with the neo-classical velocities illustrated. The consequences of the measured anomalous poloidal velocity profiles applied in transport simulations are demonstrated in section 3.2. The results from various turbulence simulations of studies of the possible sources for the anomalous poloidal velocity are presented in section 3.3. Finally, section 4 presents a summary of the results and conclusions.

2. TOROIDAL MOMENTUM TRANSPORT IN JET

2.1 GLOBAL MOMENTUM AND ENERGY CONFINEMENT TIMES

It has been reported in several large tokamaks that the toroidal momentum confinement time τ_f is very similar to the energy confinement time τ_E [3,4,5]. This similarity $\tau_E/\tau_\phi \sim 1$ is further confirmed on JET for high density ($n_{el} > 15\times10^{19}\mathrm{m}^{-2}$) ELMy *H*-mode discharges, as illustrated in figure 1(a). The JET momentum transport database consists [6] of a large dataset from various JET plasma scenarios, such as ELMy *H*-mode, hybrid, *L*-mode and ITBs. τ_E/τ_ϕ and τ_E are defined as the total momentum content divided by the torque and total energy content divided by the total heating power, respectively. On the other hand, at low density ($n_{el} < 10\times10^{19}\mathrm{m}^{-2}$) a clear deviation by a factor of 1.5–3 in the equality of the two confinement times is observed as momentum confinement becomes smaller than the energy confinement $\tau_E/\tau_\phi = 1.5$–3. However, as different scenarios have typically different level of density, the effect of plasma scenarios cannot be completely excluded as clearly for example plasmas with ITB exhibit larger ratios than plasmas in the ELMy *H*-mode scenario. Still, within one scenario, there seems to be always a trend towards higher τ_E/τ_ϕ ratios at lower density.

Taking a subset of the previous discharges with accurate enough Z_{eff} measurements, one can plot similarly the ratio of the confinement times as a function collisonality parameter ν^*, shown in figure 1(b). The ratio of the energy confinement time to the momentum confinement time is clearly increasing towards lower collisionalities. The trend is very interesting as the high collisonality discharges are dominated almost solely by Ion Temperature Gradient (ITG) instability while the lower density discharges usually have both ITG and Trapped Electron Modes (TEM) unstable, often TEM becoming more or more unstable towards lower collisionalities. The Weiland model

with the self-consistent treatment of toroidal momentum transport predicts that the momentum transport is lower in ITG dominated plasmas than the ion heat transport while the opposite prevails in the TEM dominated plasmas, qualitatively consistent with the trend in figure 1(a) [7, 8].

2.2 ANALYSIS OF LOCAL MOMENTUM AND ION HEAT DIFFUSIVITIES AND THE PROFILE RESILIENCE

Based on the results from studies of global momentum and energy confinement, one would expect to have equal momentum and ion heat diffusivities in high density plasmas and a momentum diffusivity exceeding that of the ion heat in low density plasmas. However, this will not be the case. As a simple, illustrative example, the local effective diffusivities can be derived using the following equations:

$$\begin{aligned} S_\phi &= \chi_\phi^{eff} \nabla\Omega \\ Q_i &= n_i \chi_i^{eff} \nabla T_i \end{aligned} \quad \Rightarrow \quad P_r = \frac{\chi_\phi^{eff}}{\chi_i^{eff}} = \frac{S_\phi}{Q_i} \frac{S_i T_i}{\Omega} \left(\frac{R/T_{Ti}}{R/T_\Omega} \right) \tag{2}$$

where Q_i and S_ϕ are the heat and torque fluxes, Ω the angular momentum density, T_i and n_i the ion temperature and density, and L_{Ti} and L_ϕ are local inverse temperature and angular momentum density gradient lengths. Here, the average gradient lengths are averaged over the region exhibing stiff ion temperature profiles, typically from $\rho = 0.4$ to $\rho = 0.7$. However, in order to improve the accuracy, one can calculate the diffusivities using a transport code in an interpretive way, with self-consistent calculation of power deposition and torque density profiles. In this work, the JETTO transport code has been used [9]. This ratio is shown in figure 2 for 9 very high density *H*-mode discharges (red triangles, same as in figure 1), 8 other *H*-mode pulses with $T_i = T_e$ (black circles) and 25 other *H*-mode pulses with $T_i \neq T_e$ (blue circles). The effective diffusivities are averaged over the gradient region between $\rho = 0.4$ and $\rho = 0.7$.

It is to note that the ratio $\chi_\phi/\chi_i = 0.1–0.4$ is valid for all analysed *H*-mode discharges. This number is smaller than $\chi_\phi/\chi_i = 1$, commonly used in ITER predictions and often appearing in the ITG theory [10]. At first sight, there also seems to be an obvious discrepancy between the momentum and ion heat transport with respect to global and local transport properties. Looking into the different terms in equation (2), the ratio of the normalised gradient lengths L_{Ti}/L_Ω is typically close to or just below one. However, the ratio of the normalised torque flux to the heat flux $S_\phi/Q_i \times T_i n_i/\Omega$ is always below one, around 0.2–0.4 for all discharges in the database. This ratio can be understood when comparing the ion, electron and torque deposition profiles, where it is obvious that the ion heating power is deposited more centrally than the torque and the electron heating power, thus giving rise to the small ratio of $S_\phi/Q_i \times T_i n_i/\Omega$. This is most pronounced in the high density plasmas where the torque density profile can peak as out as at $\rho = 0.8$. What is not clear at firstly sight is why locally in the gradient region $\chi_\phi/\chi_i = <1$ is true while globally $\tau_E/\tau_\phi \geq 1$ takes place. However, the database indicates that while the core transport is smaller for v_ϕ, the pedestal momentum confinement is worse than that of ion heat and in

fact, the edge pedestal is weaker for momentum than for the ion temperature. In addition, as lower density discharges tend to have stronger T_i pedestal, the global energy confinement becomes better due to profile stiffness with decreasing density while the global momentum confinement does not as the toroidal rotation profile does not exhibit any stiffness, as illustrated in figure 3.

What is shown in figure 3 (a) is quite a typical observation in high density high power ELMy *H*-mode discharges, i.e. after a short ELM free period there is a giant ELM that collapses the pedestal values of temperatures, density and toroidal velocity. Looking into the logarithmic ion temperature profile one can see that the logarithmic gradient is the same over large radius from R≈3.4m to R≈3.7m before and after the ELM. This is a well-known feature called profile stiffness or profile resilience [11]. This is true both before the ELM crash and after it, i.e. the ELM crash in T_i profile propagates fast into the core region. However, the things are quite different for the logarithmic toroidal velocity profile. Firstly, there is no region of constant gradient before or after the ELM. And secondly, the ELM crash occurring in the pedestal does not propagate into the core in its full strength. Both of these observations demonstrate strongly that the profile stiffness does not exist for v_f. From the theoretical point of view, this has been expected as the drive of the ITG/TEM turbulence does not depend on the gradient length of v_f, except at very high values of [12, 13].

2.3 Transport Simulations of Toroidal Momentum Transport

An extensive transport modelling study has been performed for high and low density ELMy *H*-mode discharges, hybrid scenario discharges and *L*-mode discharges. A new version of the Weiland model that includes self-consistent treatment of the toroidal velocity has been developed. A comparison of the toroidal velocity, ion and electron temperatures and ion heat diffusion coefficients between the experiment and predictions with the new version of the Weiland model as well as with GLF23 transport model [14, 15] is illustrated for one typical high density ELMy *H*-mode discharge in figure 4. The turbulent modes for this high density, high collisionality discharge are expected to be completely ITG dominant and this is also confirmed with the linear gyrokinetic flux tube code KINEZERO [16]. The agreement between the predictions with both models and the experimental profiles is very good and of the same accuracy as the predictions for the temperatures. This kind of good agreement of v_ϕ and T_i between the predictions and experiments is generally true for other transport simulations of high density ELMy *H*-mode discharges existing in the JET momentum database. Both models also predict that the ratio of χ_ϕ/χ_i is around 0.2–0.5 in the gradient region, consistently with interpretive local transport analysis of the diffusivities presented in section 2.2.

For the ITB plasmas, both the GLF23 and the Weiland model cannot usually reproduce the profiles satisfactorily [17]. Consequently, the Bohm/gyroBohm model with the empirical ITB threshold condition [17] and with the assumption of $\chi_\phi = 0.4\,\chi_i$ has been used to predict the toroidal velocity profile together with the temperature and density profiles. This is illustrated in figure 5. In this case the agreement of the toroidal velocity profile is closer to the experimental one than that of the temperatures, but generally, the agreement of the toroidal velocity in ITB plasmas is of the same

accuracy as that of the temperatures when using the Bohm/gyroBohm model with the assumption of $\chi_\phi = 0.4\,\chi_i$.

3. POLOIDAL VELOCITY IN JET ITB PLASMAS

3.1 EXPERIMENTAL RESULTS OF POLOIDAL VELOCITIES IN ITB PLASMAS

The experimental ion temperature, density and toroidal and poloidal velocities are shown in figure 6 for a typical JET ITB discharge at four instants. The poloidal velocities can reach values of up to $v_\theta = -50$km/s within the fully developed ITB while before ITB formation they stay around 5-10 km/s. A negative value of v_θ is defined to flow in the ion diamagnetic drift direction. The comparison between carbon poloidal velocity v_θ and the neoclassical predictions for the carbon ion velocity calculated with the neo-classical transport code NCLASS [18] is shown in figure 7 (left frames) for two JET discharges. The measured carbon v_θ is an order of magnitude larger within the ITB than its neo-classical estimate for both cases. Even the sign of the measured carbon v_θ is different from the neo-classical one in some radial regions, and furthermore, can change sign within the ITB. Similar results are obtained for other JET ITB discharges [19]. Due to the large difference in v_θ between the measured value and the neo-classical estimate, the evaluated radial electric field E_r (from equation (1)) depends thus on the source of v_θ and is in most cases much larger when the measured v_q is used instead of the neo-classical one, as shown in figure 7 (right frames). In particular, even if the absolute value of E_r is not always larger when using the measured v_θ, the $E{\cdot}B$ flow shear within the ITB certainly is significantly larger, as discussed further in next section.

3.2 PREDICTIVE TRANSPORT MODELLING OF ITB PLASMAS USING THE MEASURED POLOIDAL VELOCITIES

Predicting the dynamics of the ITBs has turned out to be one of the biggest challenges for transport models. In particular the first-principle transport models often fail to predict the onset of the ITB or the radial location correctly [17]. There are most probably several reasons for having difficulties in reproducing ITBs, but one of the reasons, not taken into account earlier is that past transport simulations have always assumed that the poloidal rotation velocity is neo-classical. As shown earlier, this is not a good assumption and therefore, the used $E{\times}B$ flow shear in the transport simulations has not been appropriate.

In order to illustrate the changes in the modelling results due to the different source of v_θ two predictive simulations, both with the Weiland transport model and GLF23 are compared for JET ITB Pulse No: 59193 in figure 8. The only difference between the two simulations with both models is that the first ones (blue dotted in the case of Weiland and green long- dashed of GLF23) use the neo-classical poloidal velocity from NCLASS whereas the second ones (magenta short-dashed in the case of Weiland and yellow dash-dotted of GLF23) employ the experimentally measured v_θ in the calculation of E_r and $\omega_{E\times B}$ flow shearing rate. In all the cases, the simulations are run from $t = 5.0$s until $t = 6.8$s, covering thus the phase without an ITB roughly before $t = 6$s, towards the ITB formation phase and

until the ITB sustainment phase. All the initial conditions, and boundary conditions on top of the *H*-mode pedestal taken from the experimental data from Pulse No. 59193 at t = 5.0s. The q-profile is rather flat in the core region (slightly reversed in the very centre well inwards from the location of the ITB), and thus the negative magnetic shear does not act as the main mechanism to form the ITB for this pulse. Instead, the q = 2 surface is believed to play a significant role in triggering the ITB for this discharge as for many other JET ITB pulses on JET [20, 21].

The Weiland model and GLF23 predict the ion and electron temperature profiles well in the phase before the ITB has formed with both options of poloidal velocity. In the case when the experimental poloidal rotation is used, the Weiland model predicts the ion ITB just at the right radial location and right instant with roughly the same ITB strength as measured in the experiments. And the same is true also in the case of GLF23. On the other hand, otherwise identical simulations except with v_θ from NCLASS does not exhibit any sign of an ITB in either case and the agreement in T_i and T_e is much worse. Worth noting are also the large differences in E_r as a strong well appears at the location of the ITB with measured v_θ instead of a gentle hill with neo-classical $v_{\theta.}$ Furthermore, the $\omega_{E\times B}$ shearing rates are locally by an order of magnitude larger thanks to the deep E_r well with measured poloidal velocity. This clearly demonstrates that one of biggest deficits in transport simulations of ITB plasmas has been the lack of knowledge of v_θ, leading further to the wrong estimate for the $\omega_{E\times B}$ shearing rates. However, using the measured poloidal velocities does not necessarily improve our predictive capabilities to model ITBs although now when imposing more experimental data, we can form ITBs. In order to genuinely improve our predictive capabilities, one should also be able to predict the increase in v_θ self-consistently rather than using the experimentally measured data.

3.3 TURBULENCE SIMULATIONS OF THE GENERATION OF THE POLOIDAL ROTATION VELOCITY

As shown earlier, the measured poloidal velocity is certainly not neo-classical and indeed, significantly affects the predictions of the transport simulations. However, the cause for the difference between measured and neo-classical v_θ, i.e. the source of the anomalous poloidal velocity, is not fully clear at present. Generation of the poloidal flow has been studied with two different turbulence codes; the TRB turbulence code [22] that solves fluid equations for ITG/TEM turbulence and with non-linear 3D global electromagnetic fluid turbulence code CUTIE [23]. The time evolution of the deuterium poloidal velocity v_θ in those turbulence codes can be written as in equation (3)

$$\frac{\delta\langle v_\theta\rangle}{\delta t} = -\nu_{NC}\left(\langle v_\theta\rangle - \langle \mu_{NC}\rangle\right) - \frac{\delta}{r^2\delta r}\left\langle r^2 \nu_{E,\theta}\nu_{E,r}\right\rangle + \frac{\langle jB\rangle}{m_i n_i} + \frac{\langle S_{NBI,\theta}\rangle}{m_i n_i}, \qquad (3)$$

where ν_{NC} represents the neo-classical viscous damping term, u_{NC} is the neo-classical poloidal rotation velocity, $\Pi_{RS}=<\nu_{E,\theta}\nu_{E,r}>$ is the Reynolds stress, $\left\langle \tilde{j}\tilde{B}\right\rangle/m_i n$ the Maxwells stress and $S_{NBI,\theta}$ represents the source (torque) from the NBI in the poloidal direction. However, the experiments

show no evidence on any clear correlation between the changes in v_θ after changes in the NBI power, indicating that the last term is small and thus will not be considered later nor it is taken into account in TRB or CUTIE. TRB also neglects the electro-magnetic term (Maxwell stress).

In general, the poloidal velocity v_θ is supposed to be damped to the neo-classical level u_{NC} because of the large neo-classical viscous damping term ν_{NC}, proportional to ion-ion collisions. The orbit squeezing effect due to large temperature and density gradient may, however violate the neo-classical theory and thus could decrease ν_{NC}. On the other hand, the orbit squeezing effect in these plasmas (the gradients are not of extreme nature) is not expected to be large enough to explain the difference of an order of magnitude between the measured and neo-classical carbon poloidal velocity.

Consequently, the main candidate to explain the anomalous v_θ is thought to be the turbulence driven poloidal velocity through the Reynold's and Maxwell's stresses. For standard ITG turbulence, the quasi-linear expression of the Reynolds stress can be written as

$$\Pi_{RS,QL} = \mu\delta_r V_E \quad ; \mu = 2\,\frac{T_D}{T_e}\,\frac{q}{|k_\theta s\rho_D|}\,\frac{L_p}{\nu_{TD}}\,\langle|\nu_E|^2\rangle \tag{4}$$

where $V_E = -E_r/B$ is the $E\times B$ drift poloidal velocity, $\overline{k_\theta}$ is an average poloidal wavenumber, ρ_D and v_{TD} are the deuterium Larmor radius and thermal velocity, L_p the pressure gradient length, and s is the magnetic shear. The relationship between V_E and v_q is given by the force balance equation (1). Solving equation (3) in steady-state, one can see that the influence of turbulence appears as a negative-viscosity effect when the 2nd order differential equation is solved for V_E.

Using the simple expression (4) without turbulence, $\mu=0$, the standard neoclassical value for V_E is recovered and v_θ approaches u_{NC} within the neo-classical damping ν_{NC} frequency. Note also that for a large value of μ, V_E becomes small and v_θ is found to be in the electron diamagnetic direction for a large enough co-rotating toroidal velocity ($qv_\phi>0$). For small toroidal velocities, v_θ is rather directed in the ion diamagnetic direction.

Simulations with the TRB code of a plasma with $\rho_*=0.01$ (standard H-mode plasma with no ITB) indicate a shift of the deuterium velocity in the electron diamagnetic direction of a fraction of the diamagnetic velocity, as shown in figure 9. As the deuterium poloidal velocity $v_{\theta,D}$ is almost half of its diamagnetic velocity, the carbon poloidal rotation $v_{\theta,C}$ is, according to force balance equation, significantly higher than the carbon neo-classical velocity. Consequently, it seems very plausible according to TRB that the source of the measured anomalous carbon v_θ is driven by the turbulence through the Reynold's stress even in the case without an ITB.

TRB simulations have also been performed with a reversed q-profile, leading to the onset of an ITB. Again, a large non-neoclassical poloidal velocity is observed, which is peaking strongly within the barrier, qualitatively in accordance with experimental results. This is shown in figure 10. However, it is directed in the electron diamagnetic direction, whereas for most of the JET ITB discharges v_θ is observed to be in the ion diamagnetic direction within the ITB. On the other hand, there are also discharges where the measured poloidal rotation is shifted in electron diamagnetic direction, such

as Pulse No: 61352 shown in figure 7. For the moment, we have not identified any parametric dependence for the direction of the anomalous poloidal velocity within the ITB.

Turbulence simulations to study the turbulence generation of poloidal velocity have been also performed with non-linear 3D global electromagnetic fluid turbulence code CUTIE. The simulations are carried out using the input data from Pulse No: 58094 (shown in figure 6) at $t = 5.5$s. The simulation has been run for 144ms, reaching quasi steady-state situation except the very edge. The code evolves temperatures, density, q, and toroidal and poloidal velocity profiles of the main ions (deuterium), together with turbulence.

The predicted ion and electron temperature and poloidal and toroidal velocity profiles are compared with experimental ones in figure 11. CUTIE predicts an ion ITB at $r/a = 0.4$, roughly consistent with experiment, although the temperature predictions outside the ITB are not satisfactory. This may be due to the missing trapped particle physics code, as TEM is often significant outside the ITB in low density ITB plasmas. However, more interestingly CUTIE predicts a significant peak in deuterium v_θ (green dashed curve), much higher than the neo-classical v_θ (blue dotted curve), in the inner side of the ITB flowing in the ion diamagnetic direction. CUTIE does not consider impurities directly and therefore, the direct comparison of carbon poloidal velocity between the experimental measurements and simulation is not possible. However, the red curve in figure 11 represents the poloidal $E \times B$ velocity, and this velocity is rather close to the carbon poloidal velocity as the diamagnetic velocity of carbon is low due to high Z. Although quantitatively the magnitude of the predicted poloidal velocity is in fairly good agreement with the experimental one, qualitatively CUTIE predicts the peak in v_θ at the inner side of the ITB while experimental results show the peak exactly within the ITB.

Looking back into equation (3), it is possible to study whether the peak in v_θ is generated mainly by the electro-static or electromagnetic turbulence. According to CUTIE, the electrostatic part, i.e. force due to the Reynold's stress (red dash-dotted curve) plays the dominant role in generating v_θ for this shot while the Maxwell stress gives only a minor contribution (magenta dotted curves). This is presented in figure 12 where the different poloidal force densities are plotted time-averaged over the last 30ms of the simulation shown in figure 11. This simulation result in which the Reynold's stress has been found to be the dominant contributor to the generation of the anomalous v_θ at the strong JET ITBs is consistent with TRB results where anomalous v_θ is predicted purely with Reynold's stress (without electro-magnetic turbulence). For a comparison there is also an estimation for the calculated total poloidal stress (black solid line) using equation (3), assuming steady-state and that only neo-classical damping exists, which is needed to drive the poloidal velocity up to the measured level. To be noted here is that both codes neglect the possible role of geodesic acoustic modes in flow generation.

SUMMARY AND CONCLUSIONS

Momentum transport studies using the toroidal momentum database have confirmed the earlier

observation that $\tau_E/\tau_f \sim 1$ at high density plasmas although at low density or low collisionality, τ_E becomes larger than τ_f by a factor of 1.5–3. On the other hand, locally in the gradient region a ratio of χ_ϕ / χ_i=0.1–0.4 is determined from the local interpretive transport analysis for high density ELMy *H*-mode discharges. This discrepancy in the momentum and ion heat transport between the global and local transport can be at least partly understood by the fact that the momentum pedestal is weaker than that of the temperature. The analysis of the profile stiffness studies during a giant ELM crash shows that while the ion temperature profile is very stiff as is well-known for a long time, such a profile stiffness is not observed in toroidal velocity profile. This is due to the facts that there is no region of constant gradient before or after the ELM and secondly, the ELM crash of rotation occurring in the pedestal does not propagate into the core in its full strength.

In order to extrapolate the toroidal velocities in the ITER core plasma, a reassessment is needed as the standard assumption $\chi_\phi / \chi_i = 1$ is not justified from the JET results. The self-consistent transport simulations of toroidal momentum with the Weiland model and GLF23 predict v_f roughly with the same accuracy as T_i. They also show that the condition χ_ϕ / χ_i = 0.2–0.5 is required for high density ELMy *H*-mode plasmas in order to predict simultaneously v_ϕ and T_i equally well. The Weiland model also predict an increase in χ_ϕ / χ_i towards TEM dominated plasmas, and this may partly explain the ratio τ_E/τ_f rising towards low collisionality TEM dominated or less ITG dominated plasmas. The linear gyro-kinetic calculations predict the ratio roughly $\chi_\phi / \chi_i = 0.7$ [24]. Therefore, as this is clearly larger than the ratio of the found effective diffusivities, the possible role of an inward momentum pinch needs further investigation in future. Another extension of this study is to look into the edge momentum transport to resolve the discrepancy in the Prandtl number between global and local analysis.

Anomalous carbon poloidal velocities, exceeding the neo-classical estimate by a factor of 10, are measured within the ITB on JET. This changes the calculated E_r and $\omega_{E\times B}$ shearing rates significantly, and improves the success of first-principle transport models to predict the dynamics of the ITBs. Both the Weiland model and GLF23 reproduce the onset, location and strength of the ITB well when the experimental poloidal velocity is used while they do not predict the formation of the ITB using the neo-classical poloidal velocity in time-dependent transport simulations. Consequently, the use of neo-classical poloidal velocity in the calculation of the *E*¥*B* is one of the major reasons why the first-principle transport models have not been successful in reproducing the dynamics of the ITBs.

Turbulence simulations with CUTIE and TRB codes show the generation of the anomalous poloidal velocity in the vicinity of the ITB. While TRB predicts the ITB within the ITB, CUTIE predicts the peak in v_θ just inside the ITB, and the sign of v_θ between the codes is different. The dominant drive for the anomalous v_θ is due tao poloidal force through the Reynold's stress according to CUTIE (TRB only has Reynold's' stress). The predicted poloidal force is qualitatively in agreement with the experimental observations. Major unresolved issues are the causality between anomalous $v_{\prod}$, onset of the ITB and the appearance of q_{min}=integer surface as well as the sign of v_θ, as neither the experiments nor the simulations reveal any clear parametric dependence.

REFERENCES

[1]. Burrell K.H. 1997 *Phys. Plasmas* **4** 1499.

[2]. Garofalo A.M. *et al.* 2001 *Nucl. Fusion* **41** 1171.

[3]. Zastrow K.-D. *et al.* 1998 Nucl. *Fusion* **38**†257.

[4]. Kallenbach A. *et al.* 1991 Nucl. *Fusion* **33**†595.

[5]. de Grassie J.S. *et al.* 2003 *Nucl. Fusion* **43**†142.

[6]. de Vries P.C. *et al.* 2006 *Plasma Phys. Control. Fusion* **48** 1693.

[7]. Weiland J. and Nordman H. 2006 *Proc. 33rd European Physical Society Conf. on Control. Fusion and Plasma Phys. (Rome, Italy, 19 – 23 June 2006) ECA* **30** P2.186.

[8]. Eriksson A. et al. 2007.

[9]. *Genacchi G. and Taroni A.* 1988 *JETTO: A free boundary plasma transport code (basic version) Rapporto ENEA RT/TIB 1988(5).*

[10]. Mattor N. and Diamond P. 1988 *Phys. Fluids* **31** 1180.

[11]. Garbet X. *et al.* 2004 Plasma Phys. Control. Fusion **46** 1351.

[12]. Peeters A.G. *et al.* 2006 Plasma Phys. Control. Fusion **48** B413.

[13]. Kinsey J.E., Waltz R.E. and Candy J 2005 *Phys. Plasmas* **12** 062302.

[14]. Waltz R.E. *et al.* 1997 *Phys. Plasmas* **4** 2482.

[15]. Kinsey J.E., Staebler G.M. and Waltz R.E. 2005 *Phys. Plasmas* **12** 052503.

[16]. Bourdelle C. *et al.* 2002 *Nucl. Fusion* **42** 822.

[17]. Tala T. *et al.* 2006 *Nucl Fusion* **46** 548.

[18]. Houlberg W. *et al.* 1997 *Phys. Plasmas* **4** 3231.

[19]. CrombÈ K. *et al*. 2006 *Phys. Rev. Lett*. **95** 155003.

[20]. Joffrin E.J. *et al.* 2002 *Nucl. Fusion* **42** 235.

[21]. Joffrin E.J. *et al.* 2002 *Plasma Phys. Control. Fusion* **44** 1738.

[22]. Garbet X. and Waltz R.E. 1996 *Phys. Plasmas* **3**1898.

[23]. Thyagaraja A. *et al.* 2005 *Phys. Plasmas* **12** 090907.

[24]. Peeters A.G. and Angioni C. 2005 *Phys. Plasmas* **12** 072515.

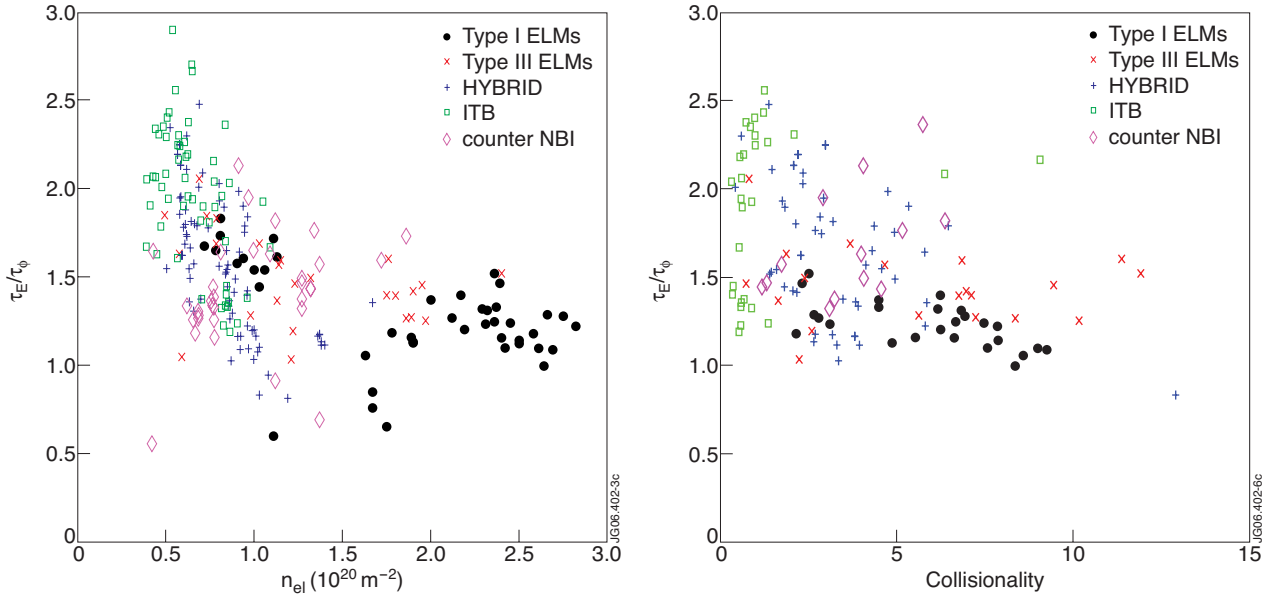

Figure 1:(a) The ratio of energy confinement time to the momentum confinement time as a function of line integrated density covering several plasma operation scenarios. (b) As in (a) but as a function of collisionality ν^*.

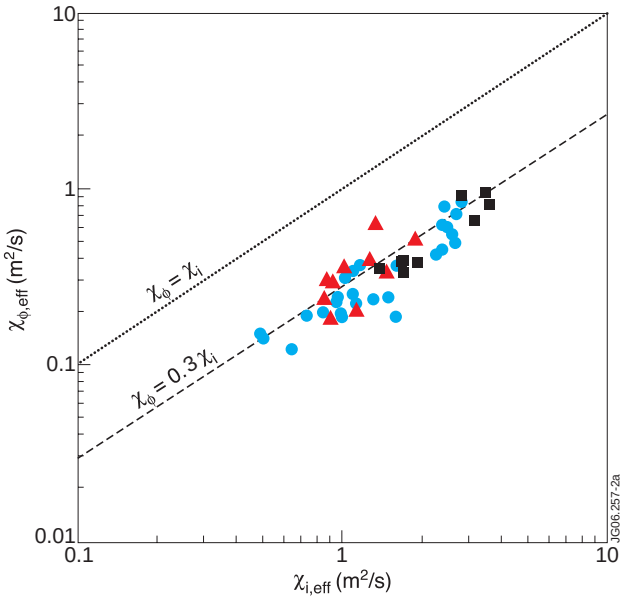

Figure 2: Effective momentum diffusivity versus effective ion heat diffusivity for 9 very high density H-mode discharges (red triangles), 8 H-mode pulses with T_i=T_e (black circles) and 25 H-mode pulses with T_i≠T_e (blue circles).

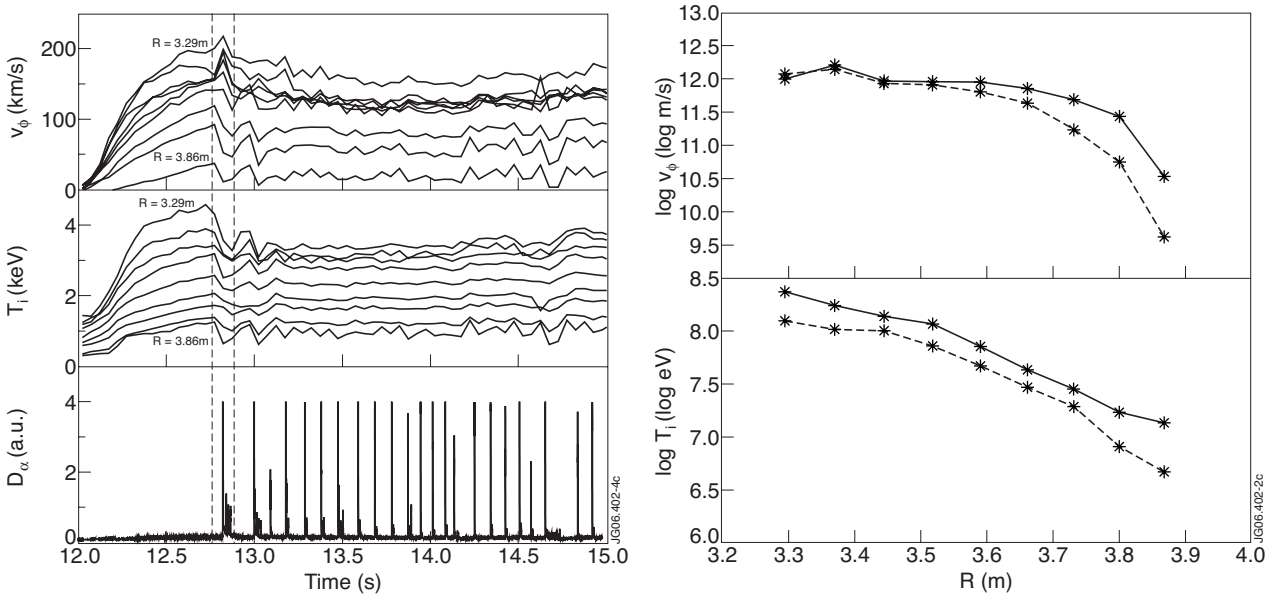

Figure 3. (a) Toroidal velocity (upper frame) and ion temperature (middle frame) traces as a function of time for several equidistant radii from R=3.29m to R=3.86m as well as D_α signal for JET Pulse No: 60870. (b) Upper frame: logarithmic toroidal velocity profile before the massive ELM crash at t=12.8s (solid curve) and after the ELM crash at t=12.9s (dashed curve) Lower frame: as in in upper frame, but for the ion temperature. The instants of the two profiles in frame (b) are indicated by the vertical dashed lines in frame (a).

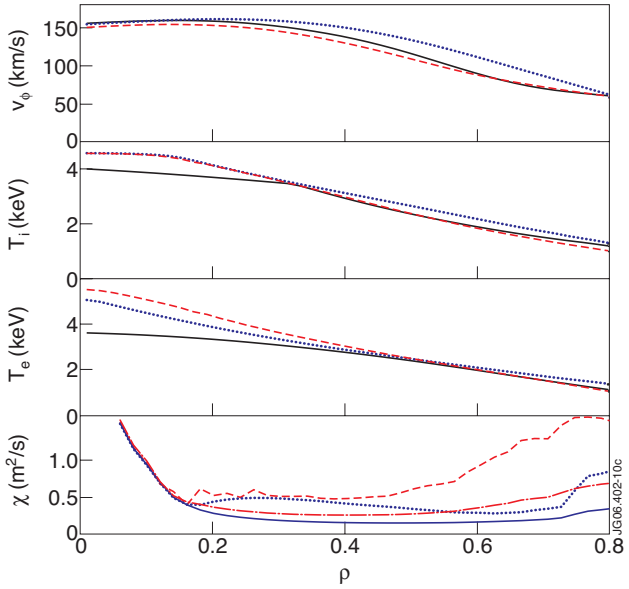

Figure 4. Experimental (solid curves) and predicted by GLF23 (dotted curves) and Weiland model (dashed curves) of v_ϕ, (upper frame), T_i (second frame) and T_e (third frame) for Pulse No: 57865. Fourth frame shows χ_ϕ and χ_i predicted by the GLF23 (blue solid and dotted curves) and by the Weiland model (red dash-dotted and dashed curves), respectively. Figure 5. Experimental (solid curves) and predicted by the Bohm/gyroBohm model (dashed curves) for all the predicted profiles for JET Pulse No: 46664.

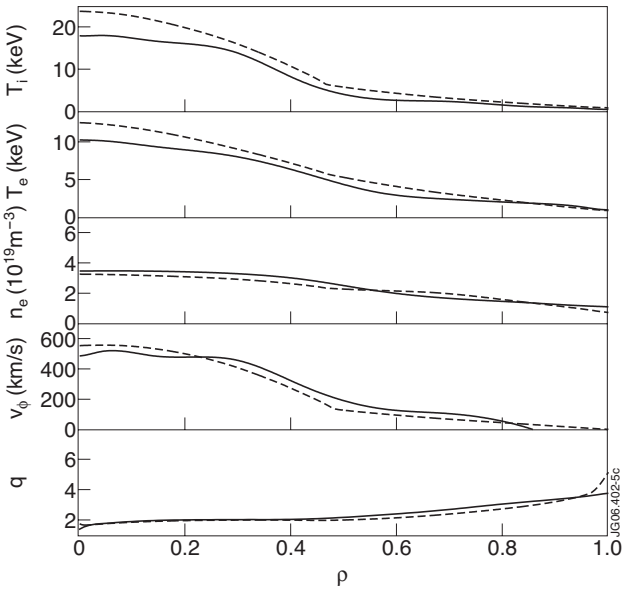

Figure 5: Experimental (solid curves) and predicted by the Bohm/gyroBohm model (dashed curves) for all the predicted profiles for JET Pulse No: 46664.

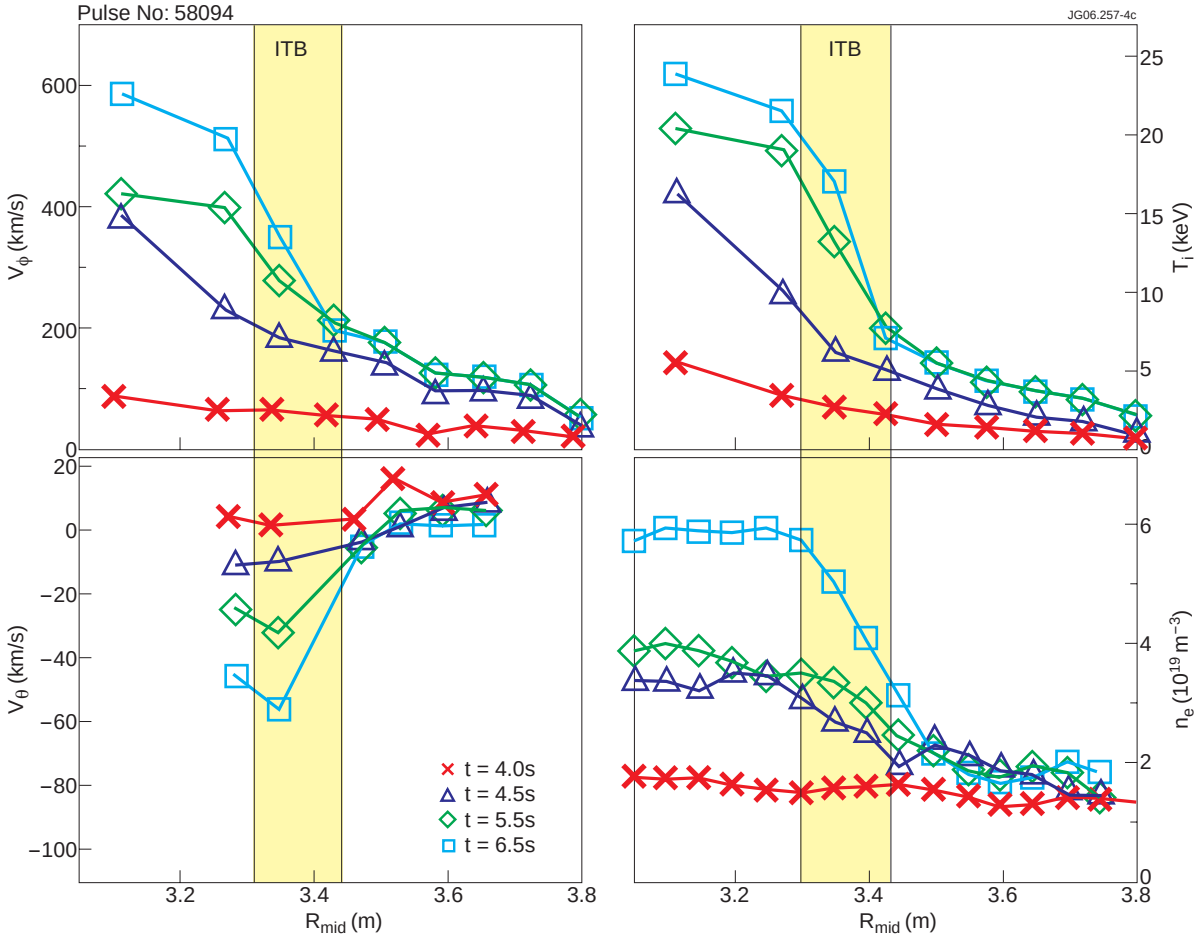

Figure 6. Toroidal and poloidal rotation, ion temperature and electron density profiles at four instants for a typical JET ITB discharge. The yellow shaded region indicates the location of the ITB.

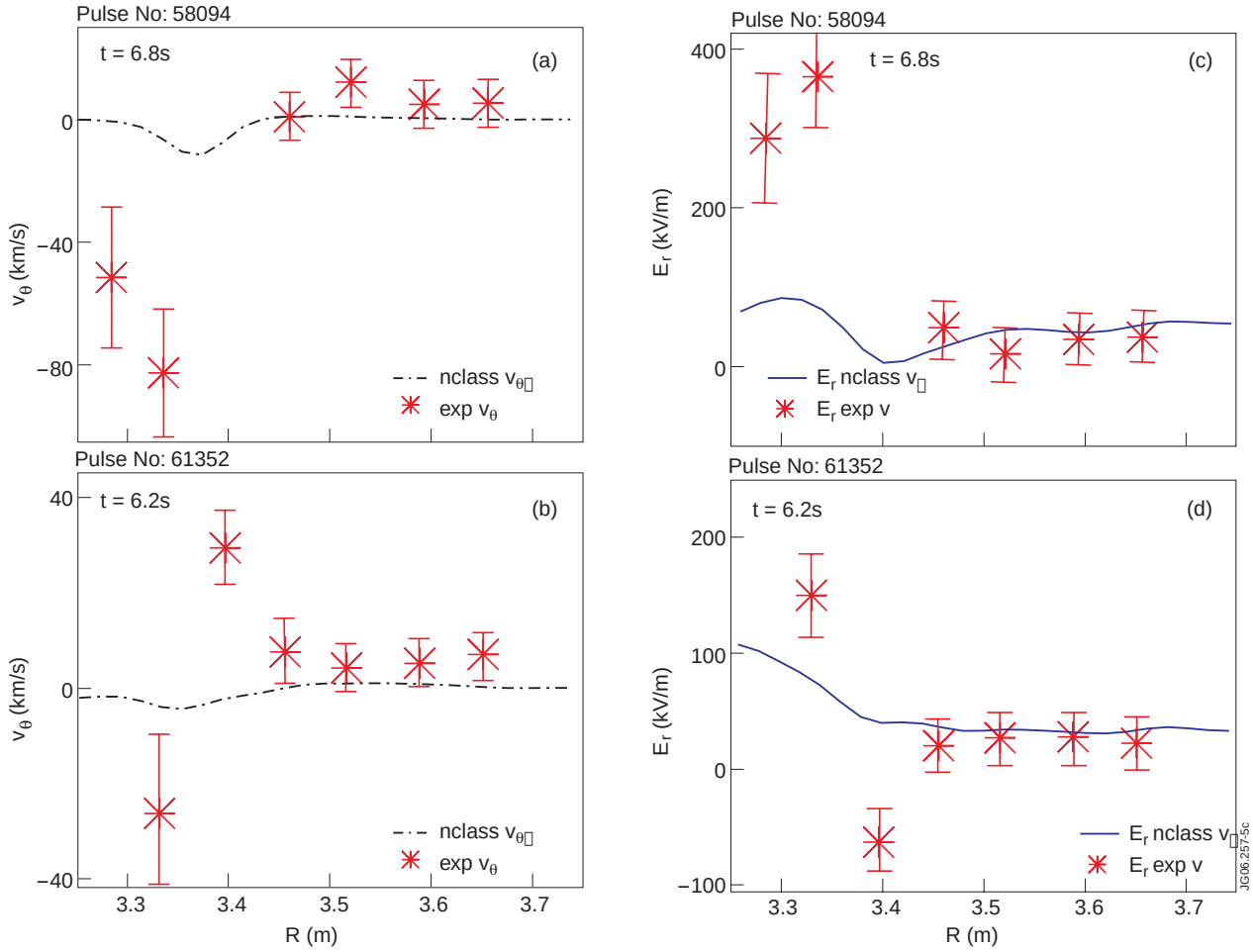

Figure 7. (a) and (b) Comparison of measured carbon v_θ profiles with neoclassical predictions by NCLASS. (c) and (d) E_r profiles calculated using the force balance equation, with the measured (stars) and the NCLASS v_θ (line).

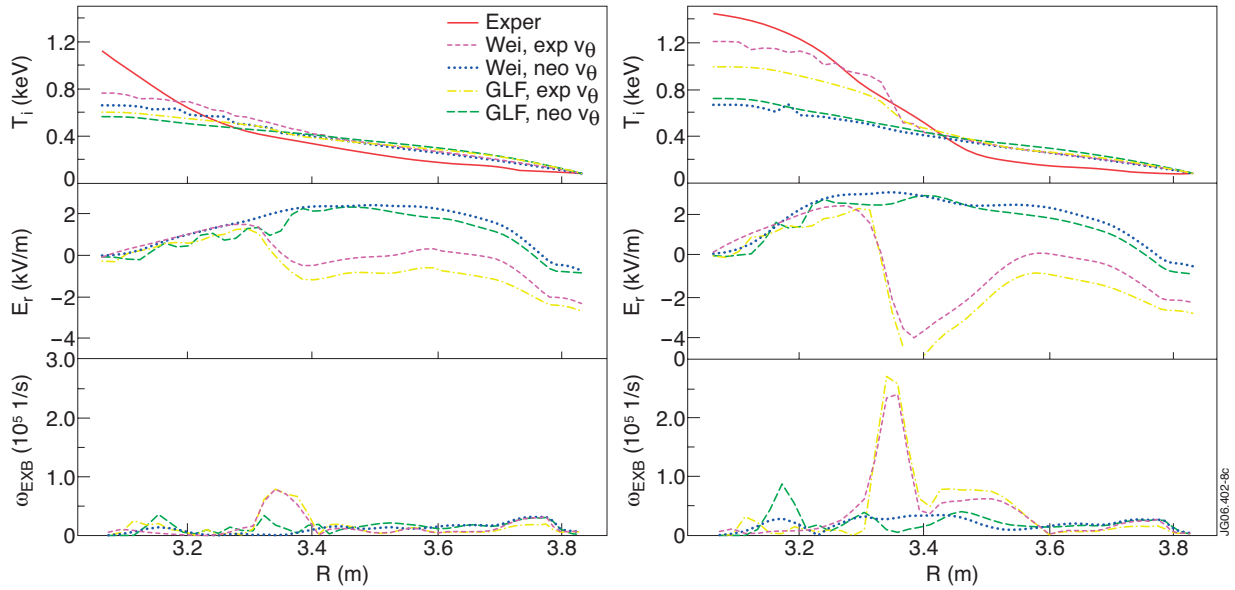

Figure 8. Predictions for the ion temperature, radial electric field and ω_{ExB} shearing rate before the ion ITB formation at t=5.7s (left frame) and after it at t=6.2s (right frame) using both the Weiland model and GLF23 either with measured or neo-classical poloidal velocity.

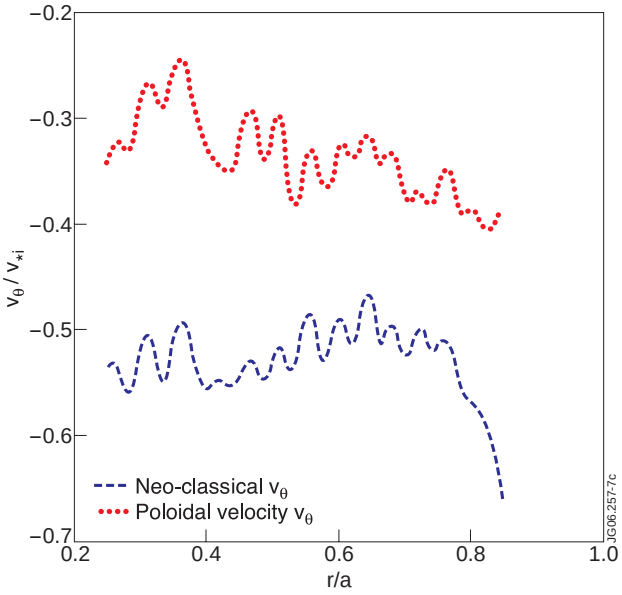

Figure 9. Radial profiles of predicted $v_{\theta,D}$ and neoclassical deuterium velocity calculated by the TRB code. The velocity unit is a diamagnetic velocity in units T/eBa and positive values are in the electron diamagnetic direction.

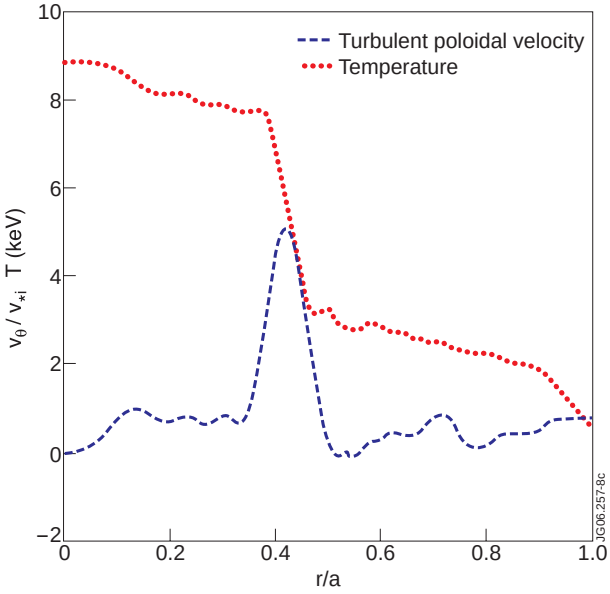

Figure 10. Radial profiles of ion temperature and the turbulent poloidal velocity (v_θ - u_{NC}) due to turbulence calculated with the TRB code for a case with a reversed q-profile. Velocity unit as in figure 9.

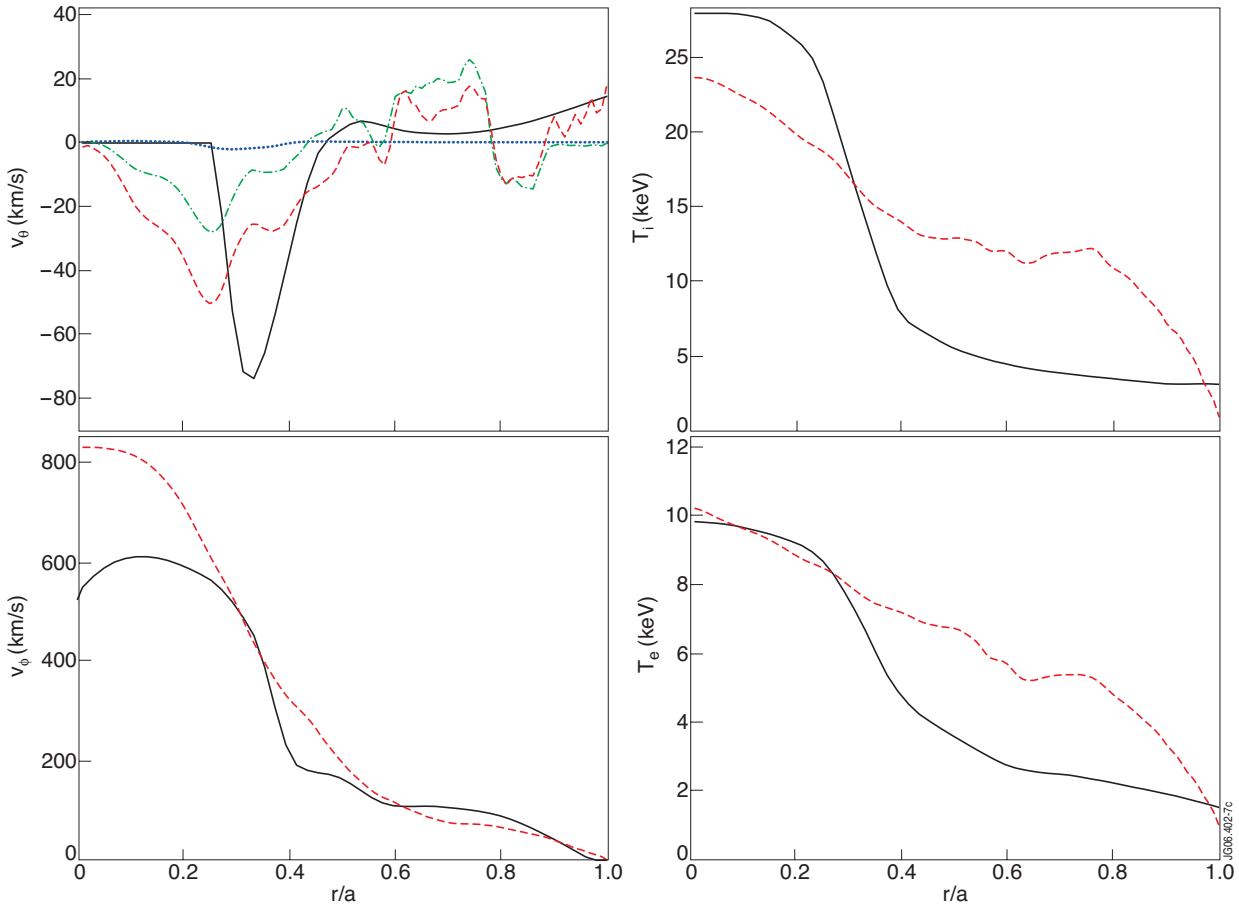

Figure 11. Comparison of v_θ, v_ϕ, T_i and T_e between the CUTIE simulation (red) and experiment (black) after 144ms simulation time for JET Pulse No: 58094 at t=5.5s. On the upper left frame, neo-the classical v_θ (blue) and the deuterium v_θ are shown as comparison while red curve represents poloidal E×B velocity, assumed to be close to carbon v_θ.

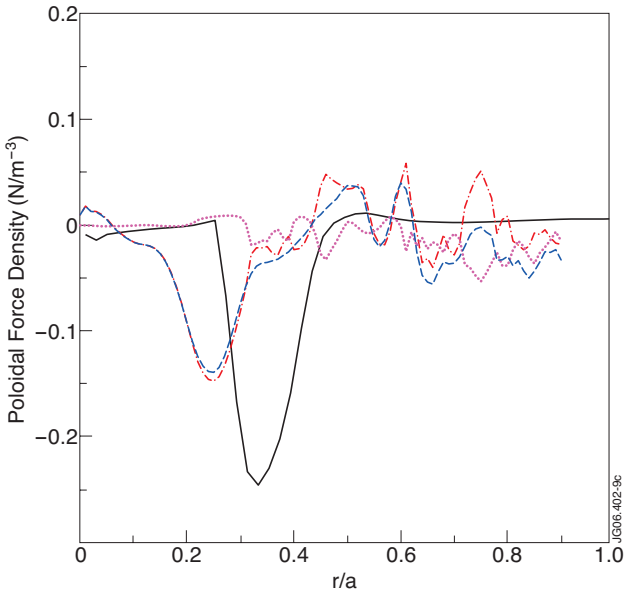

Figure 12. The poloidal force densities representing the contributions from Reynold's stress (red dash-dotted) and Maxwell's stress (magenta dotted) summing up to the total stress (blue dashed). The estimation of the total poloidal stress needed to drive the experimentally measured value is denoted by the black solid curve.